Published in final edited form as:

*Plast Reconstr Surg*. 2023 August 01; 152(2): 270e–280e. doi:10.1097/PRS.0000000000010258.

# Engineering 3D Printed Bioceramic Scaffolds to Reconstruct Critical-Sized Calvaria Defects in a Skeletally Immature Pig Model

**Evellyn M. DeMitchell-Rodriguez, MD, MS**[1], **Chen Shen, MD, MS**[1], **Vasudev Vivekanand Nayak, MSci, PhD**[2,3], **Nick Tovar, PhD, DDS**[3], **Lukasz Witek, MSci, PhD**[3,4], **Andrea Torroni, MD, PhD**[1], **Lauren M. Yarholar, MD**[5], **Bruce N. Cronstein, MD**[6], **Roberto L. Flores, MD**[1], **Paulo G. Coelho, MD, DDS, PhD, MBA**[5,7]

[1]Hansjörg Wyss Department of Plastic Surgery, New York University Grossman School of Medicine

[2]Department of Mechanical and Aerospace Engineering, New York University Tandon School of Engineering

[3]Department of Biomaterials, New York University College of Dentistry

[4]Department of Biomedical Engineering, New York University Tandon School of Engineering

[5]DeWitt Daughtry Family Department of Surgery, Division of Plastic Surgery, University of Miami Miller School of Medicine

[7]Department of Biochemistry and Molecular Biology, University of Miami Miller School of Medicine

[6]Department of Medicine, New York University Langone Health.

## Abstract

**Background:** Three-dimensional printed bioceramic scaffolds composed of 100% β-tricalcium phosphate augmented with dipyridamole (3DPBC-DIPY) can regenerate bone across critically sized defects in skeletally mature and immature animal models. Before human application, safe and effective bone formation should be demonstrated in a large translational animal model. This study evaluated the ability of 3DPBC-DIPY scaffolds to restore critically sized calvarial defects in a skeletally immature, growing minipig.

**Methods:** Unilateral calvarial defects (~1.4 cm) were created in 6-week-old Göttingen minipigs ($n$ = 12). Four defects were filled with a 1000 μm 3DPBC-DIPY scaffold with a cap (a solid barrier on the ectocortical side of the scaffold to prevent soft-tissue infiltration), four defects were filled with a 1000 μm 3DPBC-DIPY scaffold without a cap, and four defects served as

***Evellyn M. DeMitchell-Rodriguez, MD, MS***, Hansjörg Wyss Department of Plastic Surgery, New York University Langone Health, 550 1st Avenue, New York, NY 10016, evellynmdr@gmail.com.

DISCLOSURE

Dr. Coelho and Dr. Cronstein have a patent on the use of tissue repair devices and scaffolds (US20150150681A1). Dr. Cronstein holds patents 5,932,558, 6,020,321, 6,555,545, and 7,795,427. The other authors report no proprietary or commercial interest in any product mentioned or concept discussed in this article.

Disclosure statements are at the end of this article, following the correspondence information.

Related digital media are available in the full-text version of the article on www.PRSJournal.com.

negative controls (no scaffold). Animals were euthanized 12 weeks postoperatively. Calvariae were subjected to micro–computed tomography, 3D reconstruction with volumetric analysis, qualitative histologic analysis, and nanoindentation.

**Results:** Scaffold-induced bone growth was statistically greater than in negative controls ($P \leq 0.001$), and the scaffolds with caps produced significantly more bone generation compared with the scaffolds without caps ($P \leq 0.001$). Histologic analysis revealed woven and lamellar bone with haversian canals throughout the regenerated bone. Cranial sutures were observed to be patent, and there was no evidence of ectopic bone formation or excess inflammatory response. Reduced elastic modulus and hardness of scaffold-regenerated bone were found to be statistically equivalent to native bone ($P = 0.148$ for reduced elastic modulus of scaffolds with and without caps and $P = 0.228$ and $P = 0.902$ for hardness of scaffolds with and without caps, respectively).

**Conclusion:** 3DPBC-DIPY scaffolds have the capacity to regenerate bone across critically sized calvarial defects in a skeletally immature translational pig model.

**Clinical Relevance Statement:** This study assessed the bone generative capacity of 3D-printed bioceramic scaffolds composed of 100% β-tricalcium phosphate and augmented with dipyridamole placed within critical-sized calvarial defects in a growing porcine model.

Bone is the second most commonly transplanted tissue, producing an annual health care expense of approximately $2.5 billion.[1,2] Autologous bone grafts are the standard for repair of the majority of pediatric craniofacial defects. However, autologous bone transfer is limited by the need for a secondary surgical site, donor-site morbidity, extended length of stay, high associated costs, and potential graft resorption.[3,4] In addition, bone grafts are restricted by the shape and volume of available bone stock, making large or complex defects challenging to repair.[5] Alternatives to autologous bone transfer include allografts, xenografts, and synthetic materials, but these treatment options can be associated with infection, foreign body reaction, or graft fracture or extrusion.[6–8]

Bone replacement in the pediatric population is further complicated by the need for the implanted material to grow and remodel with the patient. The ideal pediatric bone replacement would restore structure and function while pre-serving normal growth. Considering the limitations of current bone replacement options, bone tissue engineering may present the ideal bone replacement in the growing craniofacial skeleton.

Some of the most common bone replacement materials are calcium phosphate–based bioactive ceramics, such as hydroxyapatite and β–tricalcium phosphate (β-TCP).[9,10] Although these ceramics are biocompatible, are osteoconductive, and have favorable safety profiles,[9,11] their slow degradation kinetics limit the amount of bone replacement occurring over time.[12] These limitations have been overcome by advances in biomaterials and computer-aided design and manufacturing, allowing for the three-dimensional (3D) printing manufacture of a bioceramic scaffold matrix that balances the needs of osteoconduction, vascularization, mechanical stability, and degradation kinetics.[13,14] Furthermore, these 3D printed scaffolds can be customized to fill any defect site precisely.[14,15] The osteogenic potential of these bone tissue engineering scaffolds can be further augmented by

osteogenic agents such as recombinant human bone morphogenic protein-2 (rhBMP-2) and dipyridamole.[14,16–18]

Previous studies, using several different animal models, have demonstrated the ability of 3D-printed bioceramic (3DPBC) scaffolds composed of 100% β-TCP to regenerate bone within critical-sized defects with bone morphology and mechanical properties that are equivalent to native bone.[17,19,20] The addition of dipyridamole, an indirect adenosine A2A receptor agonist, can further augment the osteogenic ability of these scaffolds without causing ectopic bone formation or premature growth plate fusion in growing craniofacial animal models.[16,21] The scaffold design and osteogenic agent dose has been refined to balance the needs of osteogenesis, scaffold stability, and degradation kinetics.[22] Long-term studies have demonstrated that reconstruction of critical-sized calvarial and alveolar defects with 3DPBC dipyridamole (3DPBC-DIPY) scaffolds resulted in bone regeneration that was statistically equivalent to autologous bone grafting and with no evidence of skeletal growth inhibition in a growing rabbit model.[23]

Although this previous work has provided a foundation of evidence demonstrating the effectiveness of 3DPBC scaffolds to regenerate pediatric craniofacial defects, human application requires successful implementation of this bone tissue engineering construct in a preclinical, translational animal model. Pigs are considered to be an excellent preclinical animal model because of similarities to human bone morphology, regeneration, and wound healing.[24,25] With these goals in mind, the purpose of this study was to demonstrate the ability of 3DPBC-DIPY scaffolds to regenerate bone within critical-sized calvarial defects in a skeletally immature porcine model and further optimize scaffold design for future studies.

## PATIENTS AND METHODS

### Scaffold Design and Production

The 3DPBC scaffolds were designed using computer-aided design (RoboCAD 4.5; 3D Inks LLC, Tulsa, OK) incorporating a strut and porosity size as previously described.[22] Scaffolds were designed to have diameters of 13.5, 14.0, and 14.5 mm incorporating two designs: one with a cap (Fig. 1, *above*) and one without cap (Fig. 1, *below*). The cap is a solid structure that faces the periosteal side of the scaffold, creating a barrier to prevent soft-tissue infiltration into the defect site.[26] The cap was 500 μm thick and its diameter extended 0.5 mm beyond the diameter of the porous core.

All scaffolds described in this study were composed of 100% β-TCP augmented with 1000 μm dipyridamole.[16] A concentrated β-TCP colloidal gel ink was prepared using ceramic powder, ammonium polyacrylate, deionized water, hydroxypropyl methylcellulose, and polyethyleneimine based on previously published protocols.[17,19] For the scaffolds with caps, the cap was printed first by extruding β-TCP in two concentric circles of progressively decreasing diameter. The density of the β-TCP within the cap is the same in the struts within the remainder of the scaffold. Single layers of β-TCP struts were then extruded on top of the cap to create the remainder of the scaffold. Scaffolds had 200-μm strut thickness and 500-μm pore sizes, which previously had been determined to be the favorable dimensions

for effective bone regeneration and adequate scaffold degradation kinetics.[19,22] Detailed methods of colloidal gel and 3D printing protocols used have been published.[16,19,22]

After printing, scaffolds were dried and sintered at 1100°C to eliminate impurities and achieve sufficient mechanical properties for surgical handling. [See Figure, Supplemental Digital Content 1, which shows 3DPB scaffold with a cap (*above*) and without a cap (*below*) after sintering, http://links.lww.com/PRS/F967.] The implants were then sterilized using an autoclave. Before implantation, scaffolds were immersed in 2% type I bovine collagen solution (Corning, Inc., Corning, NY) as a carrier and then augmented with 1000 μm dipyridamole.[16]

## Surgical Intervention

All surgical interventions received approval from the institutional animal care and use committee (IA16–01955) and were performed using sterile technique. Twelve skeletally immature 6-week-old Göttingen miniature pigs (weight 2.5 ± 0.8 kg) underwent surgical creation of right-sided unilateral calvarial defects. The animals were anesthetized using xylazine 1 mg/kg intramuscularly, propofol 1 to 4 mg/kg intravenously, ketamine 20 mg/kg intramuscularly, isoflurane 0.5% to 3%, and meloxicam 0.4 mg/kg intramuscularly. The right side of the animal's head was prepped using aseptic technique. Dissection over the right side of the calvaria was performed down to the periosteum. The area of the bony defect was marked using previously created custom 3D-printed circular cutting guides with a 14-mm diameter and full-thickness defects were created free-handed using a tapered fissure bur [1.6-mm diameter, part 03.000.086S (DePuy Synthes, Westchester, PA)] attached to a Synthes Electric Pen Drive (DePuy Synthes). Defects were filled with 3DPBC-DIPY scaffolds possessing the diameter that best fit the free-handed defect site (~14 ± 0.5 mm) or left empty to serve as negative controls. The scaffolds containing a cap were inset into the calvarial defect with the cap facing the ectocortical aspect of the defect. Four pigs had their defects repaired with the scaffolds with caps, four without caps, and four defects remained empty to serve as negative controls. The soft tissue was closed in a layered fashion. Animals were allowed food and water ad libitum postoperatively and were given streptomycin 0.5 g/day intramuscularly for infection prevention and meloxicam 0.4 mg/kg intramuscularly and buprenorphine 0.05 to 0.1 mg/kg subcutaneously during the first 48 hours after surgery for analgesia. After 12 weeks, animals were euthanized by anesthesia overdose and their heads were harvested by sharp dissection.

## Imaging and Micro–Computed Tomographic Analysis

After calvarial harvest, the defect sites, as well as the unoperated, contralateral side, were isolated from the calvaria using a reciprocating saw and band saw. Samples were placed in 70% ethanol and subjected to high-resolution micro–computed tomography (micro-CT) (μCT 40; SCANCO Medical, Bassersdorf, Switzerland) (Fig. 2). Imaging data were converted to digital imaging and communications in medicine (DICOM) files and imported into Amira Software (version 6.3; Visage Imaging GmbH, Berlin, Germany) for 3D reconstruction and volume analysis. Each defect site was three-dimensionally reconstructed and had uniform thresholds set for bone, scaffold, and soft tissue or empty space. The volume of bone and scaffold in the defect site was calculated as a proportion of

total volume of the defect. The volume of bone present in the unoperated contralateral side was calculated to determine the density of native bone.

## Histologic Preparation and Analysis

After volumetric analysis, samples were dehydrated in increasing concentrations of ethanol (70% to 100%) and embedded in methyl methacrylate resin. The embedded samples were cut into 250-μm-thick sections using a diamond saw (Isomet 2000; Buehler Ltd., Lake Bluff, IL). Histologic sections were chosen from the approximate center of the scaffold for consistency across samples. Sections were then glued onto acrylic slides and ground on a grinding machine (Metaserv 3000; Buehler) using continuous water irrigation and a series of silicon carbide abrasive paper until slices had a thickness of approximately 100 μm. Slides were polished using alumina to remove residual scratches. Samples were stained with Stevenel blue and van Gieson red picrofuchsin stains to differentiate soft tissue, bone, and scaffold (soft tissue is stained blue, mineralized tissue is stained red, and scaffold appears black).

Stained samples were examined using an Aperio digital histology slide scanning system (Aperio Technologies, Vista, CA). Scanned sections underwent qualitative histologic analysis including overall bone morphology, presence of haversian canals, excess inflammatory cells, suture patency, and scaffold fragmentation.

## Nanoindentation Testing and Analysis

Slides used for histology were also subjected to nanoindentation analysis on a nanoindenter (Hysitron TI 950, Minneapolis, MN) equipped with a Berkovich three-sided, diamond pyramid probe. Nine indents per specimen were performed using a previously developed loading profile with a loading rate of 60 μ*N*/s for 5 seconds followed by a constant peak load of 300 μN, termed as holding time, for 10 seconds, and sub-sequent unloading in 2 seconds to produce load–displacement curves corresponding to each area indented.[20,27] This nanoindentation testing was performed as a comparative analysis of mechanical strength (Young modulus) and hardness of bone between areas within the lattice-like nature of the scaffold and native bone present around the induced defect site. (See Figure, Supplemental Digital Content 2, which shows a schematic representation of nanoindentation testing areas on native bone and newly developed bone within the scaffold, http://links.lww.com/PRS/F968.).

Samples were first imaged followed by a scratch test to confirm the samples were indeed flat with an error in the indenter's axial displacement recorded to be less than 1 μm over a scan area of 50 μm2. Regions were assessed further for the presence of bone in the testing site, following which nine indentations were performed in a sequential manner, with each indent separated by 10 μm from each other. Tests were performed at room temperature with appropriate passive and active noise isolation and damping. The set of nine load–displacement curves were fitted using a standard model using the Hysitron TriboScan quasistatic data analysis package to compute reduced elastic modulus, $E_r$(GPa), and hardness, $H$(GPa), of bone tissue with the following formulas[20]:

$$E_r = \frac{\sqrt{\pi}}{2\sqrt{A(h_c)}}S$$

$$H = \frac{P_{max}}{A(h_c)},$$

where $S$ is the stiffness, $h_c$ is the contact depth, $P_{max}$ is the maximum force, and $A(h_c)$ is the contact area computed from the Hysitron TriboScan software.[20,28] Elastic modulus of the bone, $E_b$, was then evaluated from the obtained reduced modulus, $E_r$, using the following Hertzian contact mechanics relationship:

$$E_b = \frac{\left(1 - \upsilon_b^2\right)E_i E_r}{E_i - \left(1 - \upsilon_i^2\right)E_r},$$

where $\upsilon_b$ is the Poisson ratio of the bone and $E_i$ and $\upsilon_i$ are the elastic modulus and Poisson ratio of the indenter, respectively.[20,28–30]

### Statistical Analysis

Statistical analysis was performed using IBM SPSS (version 25.0; IBM Corp., Armonk, NY). A generalized linear mixed model was applied to evaluate statistical significance of bone volume fraction and scaffold volume fraction between groups and also was used to determine statistical significance of reduced elastic modulus and hardness values of each group. Data are presented as means and corresponding standard deviations.

## RESULTS

### CT and Micro-CT Analysis

Three-dimensional reconstruction revealed that in all negative control group samples there was no bridging bone across the defect sites (Fig. 3). The bone volume fraction of native bone was set to 100% as a reference point to evaluate the amount of bone present in the defect sites in the negative controls and scaffold groups. Calvarial defects repaired with 3DPBC-DIPY scaffolds with and without caps regenerated an average bone volume fraction (bone volume/total volume) that was 65.6% of the bone volume fraction of native bone and was significantly greater than the mean bone volume fraction of the negative controls ($P \leq 0.001$), which were found to have 5.2% of the bone volume fraction of native bone (Table 1). When examining the amount of regenerated bone in defects repaired using the two scaffold designs, defects filled with the scaffolds that had caps yielded a significantly higher bone volume fraction compared with defects repaired without caps ($P \leq 0.001$) and had an average bone volume fraction that was 84.6% that of native bone, compared with 46.5% seen in the scaffolds without caps (Figure 4, above).

Analysis of remaining scaffold in the defect site after 12 weeks revealed no statistical differences ($P = 0.287$) between scaffold groups (with or without cap) (5.0% ± 1.4% vs 3.7% ± 2.4%, respectively) (Fig. 4, *below*).

### Histologic Analysis

Qualitative histologic analysis of nondecalcified sections of bone defects in the negative control group showed a lack of bridging bone formation across all defect sites (Fig. 5). In contrast, defects that were treated with 3DPBC-DIPY scaffolds revealed the regeneration of bone that bridged the cranial defect sites (Figs. 6 and 7). The regenerated bone in both scaffold groups demonstrated intramembranous-like healing with regions of immature woven bone and mature lamellar reorganization (Figs. 6 and 7). The regenerated bone tissue had similar morphology to native bone (Fig. 8) and appeared vascularized and highly cellular, with the presence of Haversian-like canals throughout the regenerated bone. All sutures remained patent with no evidence of premature fusion or disruption. Furthermore, there was no evidence of ectopic bone formation or excess inflammation in any histologic samples.

### Nanoindentation Testing

Mechanical testing of the scaffold-regenerated bone revealed a reduced elastic modulus ($E_r$) of 6.7 ± 1.99 GPa and a hardness (H) of 0.4 ± 0.15 GPa in the scaffolds that had caps and a reduced elastic modulus of 7.1 ± 1.71 GPa and hardness of 0.4 ± 0.17 GPa in the scaffolds that did not have caps (Fig. 9). These values were not statistically different ($P = 0.694$). Likewise, the reduced elastic modulus and hardness of the scaffold-regenerated bone from the scaffolds with caps and the scaffolds without caps were found to be statistically homogenous with the native bone ($E_r$: 8.8 ± 3.29 GPa; $P = 0.148$ and $P = 0.148$, respectively; H: 0.5 ± 0.23 GPa; $P = 0.228$ and $P = 0.902$, respectively) (Fig. 9).

## DISCUSSION

Pediatric craniofacial skeletal defects pose unique challenges to current bone replacement techniques as implants must be able to repair the bony defect as well as grow or remodel with the developing skeleton. Bone tissue engineering constructs such as 3D-printed bioceramic scaffolds are viable alternatives to current reconstructive options and have the ability to overcome limitations of standard-of-care interventions, such as the need for a second surgical site, donor-site morbidity, limited graft take, and restrictions of available bone stock. In addition, 3D printing allows for the creation of customized scaffolds that can precisely fit large or complex defects that might otherwise exceed the capabilities of autologous bone grafts and other bone replacement materials.

Previous studies have demonstrated that 3DPBC scaffolds composed of β-TCP can regenerate vascularized bone across critical-sized defects in various animal models and that the osteogenic potential is augmented with the use of dipyridamole.[16,17,19,20,23] β-TCP is a favorable ceramic for a bone tissue engineering scaffold because of its biocompatibility and osteoconductive properties. Furthermore, alteration of the macroarchitecture and microarchitecture through 3D printing can accelerate degradation kinetics while maintaining

mechanical stability. In addition to decreasing the potential for implant extrusion that exists with permanent materials, the resorption of β-TCP and replacement with generated bone renders it an appealing option for pediatric bone reconstruction, as this may reduce the chances of device migration, replacement, or extrusion associated with a permanent implant.

Although 3DPBC scaffolds composed of β-TCP alone can restore critical-sized defects, the addition of dipyridamole significantly increases their osteogenic potential. The agonistic action of dipyridamole on adenosine $A_{2A}$ receptors promotes osteogenesis by increasing osteoblast differentiation, decreasing osteoclast activity, and reducing regional inflammation.[18,31,32] In addition to its documented osteogenic abilities, dipyridamole is a favorable option as an osteogenic agent because of its long history of safe clinical use as an antithrombotic and vasodilator agent in both pediatric and adult patients under the commercial name Persantine (Boehringer Ingelheim International GmbH, Ingelheim, Germany).[33–35] Dipyridamole's osteogenic properties are a relatively recent discovery, but available data suggest it may be a superior pediatric osteogenic molecule compared with other available osteogenic agents. For example, although rhBMP-2 has a high level of osteogenic capacity and remains the most extensively used osteogenic agent to date, its use in children is controversial because of its known potential for ectopic bone formation, premature suture fusion, and osteolysis.[36–38] In contrast, dipyridamole has been shown to promote statistically equivalent bone regeneration to rhBMP-2 with no evidence of similar adverse effects.[39] The favorable characteristics of β-TCP and dipyridamole, including their osteogenic potential, biocompatibility, degradation kinetics, and safety profiles, suggest their potential for pediatric craniofacial bone replacement. In this short-term study, radiographic and histologic analysis suggests preservation of the cranial sutures using the described bone tissue engineering construct. Long-term craniofacial growth studies using a pig model will be required to make a more definitive statement on the effects of dipyridamole on craniofacial growth.

This study utilized two differently constructed scaffolds: one with a solid cap, which prevents soft-tissue infiltration into the defect, and one without, open to the periosteum and soft tissue. The findings from this study suggest that scaffolds with solid caps may facilitate a greater degree of bone regeneration than scaffolds without caps. This is consistent with previously published work in rabbit models that demonstrated inferior osteogenesis in scaffold designs that allowed for the interaction between the galea aponeurotica and ossification site.[26] While the periosteum is known to possess osteogenic potential and plays an important role in bone formation, we hypothesize that the thin periosteum of this infant animal model may have been inadequately preserved during surgical intervention. Therefore, the solid cap prevented the migration of fibrous tissue into the cranial defect.

This study demonstrates that a ~1.4-cm defect in the calvaria exceeds the regenerative ability of native bone in the growing pig and thus can be defined as critical-sized. Given the small size of 6-week-old Gottingen miniature pigs, these defects incorporated a substantial portion of the calvaria relative to the size of the animal's skull. Despite the short healing time, scaffolds were able to generate bone that had areas of lamellar organization and was statistically equivalent to native bone, which is consistent with findings of mechanical testing performed in previous publications.[20,23] The bone regeneration seen in this study

appears to be more robust compared with previous studies from this group using other animal models (eg, 27.9% ± 4.1% seen in skeletally immature New Zealand White rabbits after 8 weeks), which could be due to differences in bone healing across different animal species.[22]

This study reports the first evidence of successful bone formation of this bone tissue engineering construct in a highly translational preclinical animal model. These data provide preliminary evidence that eventually can be used to transition this bone tissue engineering construct to a clinical trial. Although a previous study demonstrated that 3DPBC-DIPY scaffolds can restore calvarial and alveolar bone defects as effectively as autologous bone graft in a growing rabbit model, this is the first study to apply this construct in a growing pig model, an animal considered to be significantly more similar to humans in terms of bone morphology, repair, and wound healing.

This study has several limitations, such as the small sample size and short study duration, precluding a more robust evaluation of this tissue-engineering construct and its potential long-term effects on bone formation or resorption within the defect and its effects on facial growth. In addition, this model utilized a negative control as a comparison group instead of a standard-of-care intervention, such as autologous bone grafting. Our aim was to create a framework for future long-term studies, which are needed to better elucidate the longitudinal effects of these 3DPBC scaffolds on bone regeneration and facial growth throughout skeletal maturity and compare it with standard-of-care interventions.

## CONCLUSIONS

A 3D-printed bone tissue engineering device composed of 100% β-tricalcium phosphate and augmented by dipyridamole can effectively repair critical-sized calvarial defects in a growing pig model. Cranial sutures appear radiographically and histologically preserved by this treatment intervention.

## Supplementary Material

Refer to Web version on PubMed Central for supplementary material.

## ACKNOWLEDGMENT

This work was completed in conjunction with an ongoing institutional animal care and use committee–approved grant (National Institutes of Health–National Institute of Child Health and Human Development R33 HD090664), “Use of 3D Printing for Creation of Implantable Pediatric Devices.”

## REFERENCES

1. Pape HC, Evans A, Kobbe P. Autologous bone graft: properties and techniques. J Orthop Trauma 2010;24(Suppl 1):S36–S40. [PubMed: 20182233]
2. Amini AR, Laurencin CT, Nukavarapu SP. Bone tissue engineering: recent advances and challenges. Crit Rev Biomed Eng. 2012;40:363–408. [PubMed: 23339648]
3. Eufinger H, Leppänen H. Iliac crest donor site morbidity following open and closed methods of bone harvest for alveolar cleft osteoplasty. J Craniomaxillofac Surg. 2000;28:31–38. [PubMed: 10851671]

4. Myeroff C, Archdeacon M. Autogenous bone graft: donor sites and techniques. J Bone Joint Surg Am. 2011;93:2227–2236. [PubMed: 22159859]
5. Oppenheimer AJ, Mesa J, Buchman SR. Current and emerging basic science concepts in bone biology: implications in craniofacial surgery. J Craniofac Surg. 2012;23:30–36. [PubMed: 22337370]
6. Beaman FD, Bancroft LW, Peterson JJ, Kransdorf MJ. Bone graft materials and synthetic substitutes. Radiol Clin North Am. 2006;44:451–461. [PubMed: 16644361]
7. Shibuya N, Jupiter DC. Bone graft substitute: allograft and xenograft. Clin Podiatr Med Surg. 2015;32:21–34. [PubMed: 25440415]
8. Haugen HJ, Lyngstadaas SP, Rossi F, Perale G. Bone grafts: which is the ideal biomaterial? J Clin Periodontol. 2019;46(Suppl 21):92–102. [PubMed: 30623986]
9. Inzana JA, Olvera D, Fuller SM, et al. 3D printing of composite calcium phosphate and collagen scaffolds for bone regeneration. Biomaterials 2014;35:4026–4034. [PubMed: 24529628]
10. Simon JL, Michna S, Lewis JA, et al. In vivo bone response to 3D periodic hydroxyapatite scaffolds assembled by direct ink writing. J Biomed Mater Res A. 2007;83:747–758. [PubMed: 17559109]
11. U.S. Food and Drug Administration, Department of Health and Human Services. Dental devices; reclassification of tricalcium phosphate granules and classification of other bone grafting material for dental bone repair. Final rule. Fed Regist 2005;70:21947–21950. [PubMed: 15858911]
12. Moore WR, Graves SE, Bain GI. Synthetic bone graft substitutes. ANZ J Surg. 2001;71:354–361. [PubMed: 11409021]
13. Shen C, Witek L, Flores RL, et al. Three-dimensional printing for craniofacial bone tissue engineering. Tissue Eng Part A. 2020;26:1303–1311. [PubMed: 32842918]
14. Lopez CD, Witek L, Torroni A, et al. The role of 3D printing in treating craniomaxillofacial congenital anomalies. Birth Defects Res. 2018;110:1055–1064. [PubMed: 29781248]
15. Witek L, Colon RR, Wang MM, et al. Tissue-engineered alloplastic scaffolds for reconstruction of alveolar defects. In: Handbook of Tissue Engineering Scaffolds: Volume One. Philadelphia: Elsevier; 2019:505–520.
16. Lopez CD, Diaz-Siso JR, Witek L, et al. Dipyridamole augments three-dimensionally printed bioactive ceramic scaffolds to regenerate craniofacial bone. Plast Reconstr Surg. 2019;143:1408–1419. [PubMed: 31033822]
17. Bekisz JM, Flores RL, Witek L, et al. Dipyridamole enhances osteogenesis of three-dimensionally printed bioactive ceramic scaffolds in calvarial defects. J Craniomaxillofac Surg. 2018;46:237–244. [PubMed: 29292126]
18. Ishack S, Mediero A, Wilder T, Ricci JL, Cronstein BN. Bone regeneration in critical bone defects using three-dimensionally printed β-tricalcium phosphate/hydroxyapatite scaffolds is enhanced by coating scaffolds with either dipyridamole or BMP-2. J Biomed Mater Res B Appl Biomater. 2017;105:366–375. [PubMed: 26513656]
19. Lopez CD, Diaz-Siso JR, Witek L, et al. Three dimensionally printed bioactive ceramic scaffold osseoconduction across critical-sized mandibular defects. J Surg Res. 2018;223:115–122. [PubMed: 29433862]
20. Tovar N, Witek L, Atria P, et al. Form and functional repair of long bone using 3D-printed bioactive scaffolds. J Tissue Eng Regen Med. 2018;12:1986–1999. [PubMed: 30044544]
21. Witek L, Alifarag AM, Tovar N, et al. Repair of critical-sized long bone defects using dipyridamole-augmented 3D-printed bioactive ceramic scaffolds. J Orthop Res. 2019;37:2499–2507. [PubMed: 31334868]
22. Maliha SG, Lopez CD, Coelho PG, et al. Bone tissue engineering in the growing calvaria using dipyridamole-coated, three-dimensionally-printed bioceramic scaffolds: construct optimization and effects on cranial suture patency. Plast Reconstr Surg. 2020;145:337e–347e.
23. Wang MM, Flores RL, Witek L, et al. Dipyridamole-loaded 3D-printed bioceramic scaffolds stimulate pediatric bone regeneration in vivo without disruption of craniofacial growth through facial maturity. Sci Rep. 2019;9:18439. [PubMed: 31804544]
24. McGovern JA, Griffin M, Hutmacher DW. Animal models for bone tissue engineering and modelling disease. Dis Model Mech. 2018;11:dmm033084.

25. Li Y, Chen SK, Li L, Qin L, Wang XL, Lai YX. Bone defect animal models for testing efficacy of bone substitute biomaterials. J Orthop Translat. 2015;3:95–104. [PubMed: 30035046]
26. Fama C, Kaye GJ, Flores R, et al. Three-dimensionally-printed bioactive ceramic scaffolds-construct effects on bone regeneration: a pilot study. J Craniofac Surg. 2021;32:1177–1181. [PubMed: 33003153]
27. Baldassarri M, Bonfante E, Suzuki M, et al. Mechanical properties of human bone surrounding plateau root form implants retrieved after 0.3–24 years of function. J Biomed Mater Res B Appl Biomater. 2012;100:2015–2021. [PubMed: 22865766]
28. Doerner MF, Nix WD. A method for interpreting the data from depth-sensing indentation instruments. J Mater Res. 1986;1:601–609.
29. Hoffler CE, Guo XE, Zysset PK, Goldstein SA. An application of nanoindentation technique to measure bone tissue Lamellae properties. J Biomech Eng. 2005;127:1046–1053. [PubMed: 16502646]
30. Lee K-L, Sobieraj M, Baldassarri M, et al. The effects of loading conditions and specimen environment on the nanomechanical response of canine cortical bone. Mater Sci Eng C. 2013;33:4582–4586.
31. Lopez CD, Bekisz JM, Corciulo C, et al. Local delivery of adenosine receptor agonists to promote bone regeneration and defect healing. Adv Drug Deliv Rev. 2019;146:240–247. [PubMed: 29913176]
32. Bekisz JM, Lopez CD, Corciulo C, et al. The role of adenosine receptor activation in attenuating cartilaginous inflammation. Inflammation 2018;41:1135–1141. [PubMed: 29656316]
33. Dengler R, Diener HC, Schwartz A, et al. ; EARLY Investigators. Early Treatment with Aspirin plus Extended-Release Dipyridamole for Transient Ischaemic Attack or Ischaemic Stroke within 24 h of Symptom Onset (EARLY trial): a randomised, open-label, blinded-endpoint trial. Lancet Neurol. 2010;9:159–166. [PubMed: 20060783]
34. McGrath LB, Gonzalez-Lavin L, Eldredge WJ, Colombi M, Restrepo D. Thromboembolic and other events following valve replacement in a pediatric population treated with antiplatelet agents. Ann Thorac Surg. 1987;43:285–287. [PubMed: 3827372]
35. Ueda N, Kawaguchi S, Niinomi Y, et al. Effect of dipyridamole treatment on proteinuria in pediatric renal disease. Nephron 1986;44:174–179. [PubMed: 3785481]
36. Spiro AS, Beil FT, Baranowsky A, et al. BMP-7-induced ectopic bone formation and fracture healing is impaired by systemic NSAID application in C57BL/6-mice. J Orthop Res. 2010;28:785–791. [PubMed: 20063306]
37. Kinsella CR Jr., Cray JJ, Durham EL, et al. Recombinant human bone morphogenetic protein-2-induced craniosynostosis and growth restriction in the immature skeleton. Plast Reconstr Surg. 2011;127:1173–1181. [PubMed: 21364420]
38. Carragee EJ, Hurwitz EL, Weiner BK. A critical review of recombinant human bone morphogenetic protein-2 trials in spinal surgery: emerging safety concerns and lessons learned. Spine J. 2011;11:471–491. [PubMed: 21729796]
39. Lopez CD, Coelho PG, Witek L, et al. Regeneration of a pediatric alveolar cleft model using three-dimensionally printed bioceramic scaffolds and osteogenic agents: comparison of dipyridamole and rhBMP-2. Plast Reconstr Surg. 2019;144:358–370. [PubMed: 31348344]

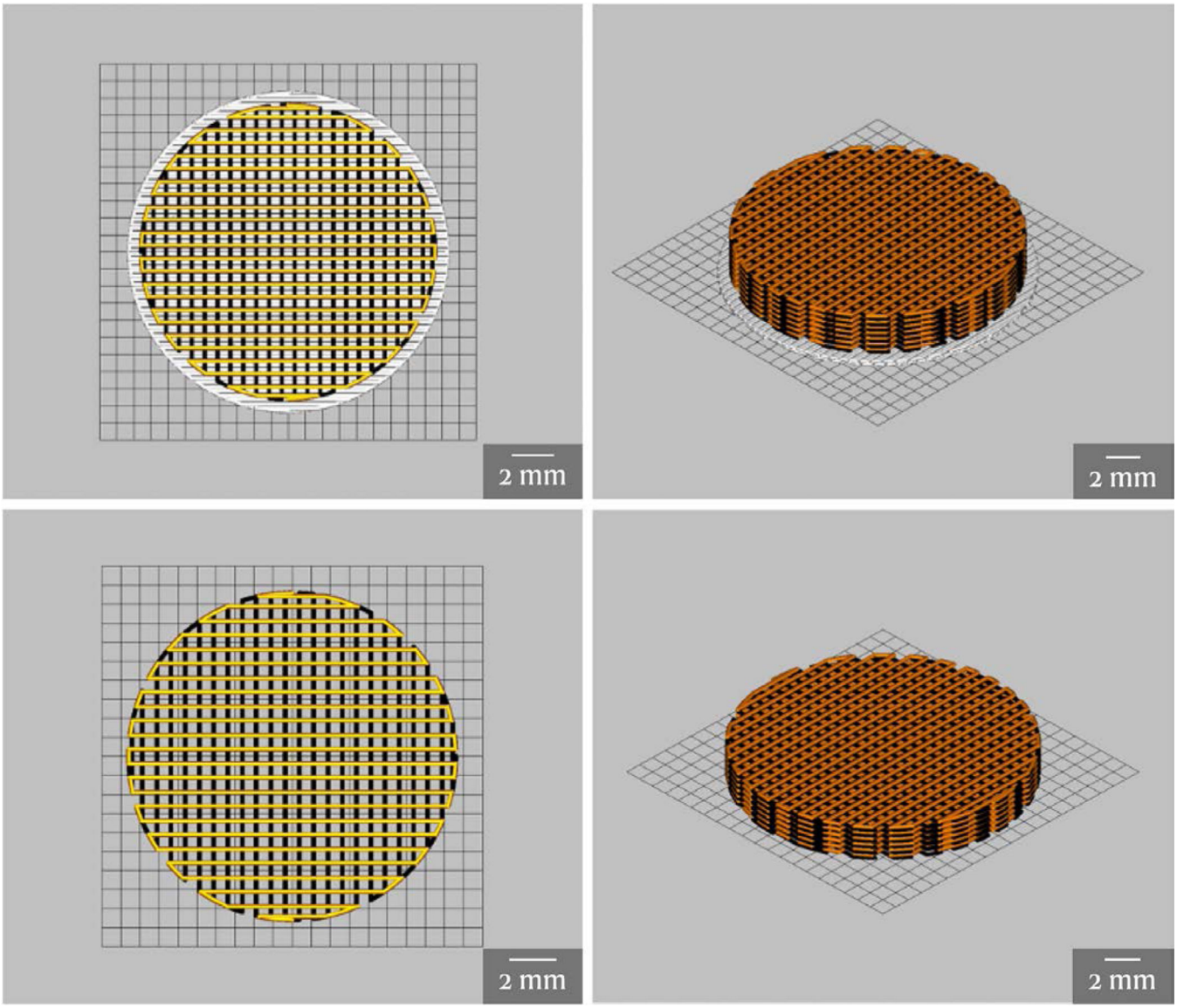


**Fig. 1.**

Schematic depiction of computer-aided design of a scaffold with a cap (*above*) and a scaffold without a cap (*below*).

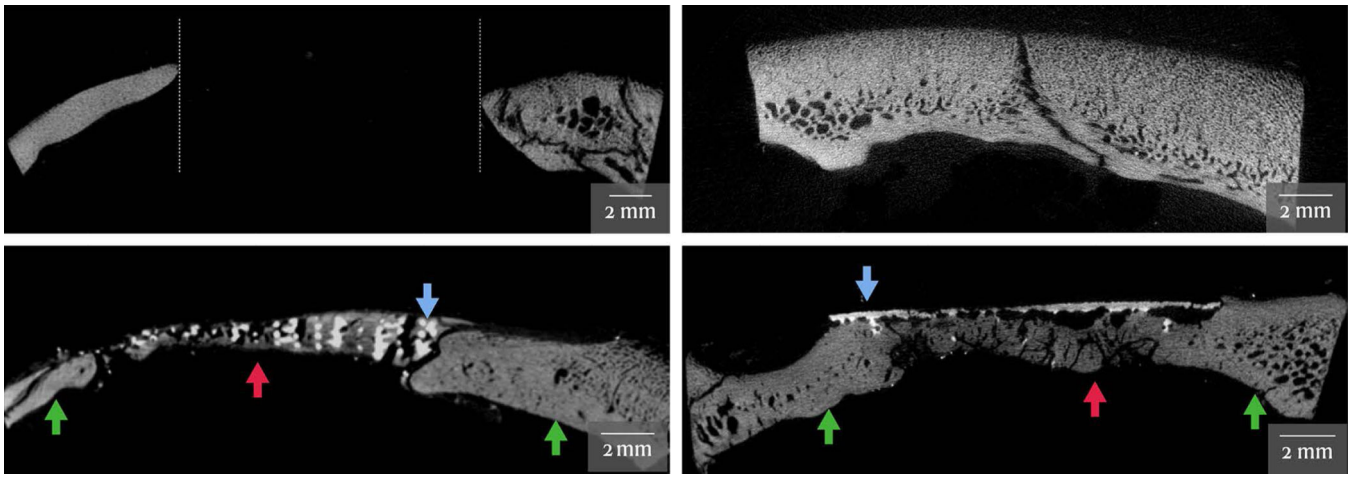


**Fig. 2.**

Micro–computed tomographic images of cross-section of the defect after 12 weeks of healing. (*Above, left*) The negative control with no bridging bone formed across the defect site (*white dashed lines*). (*Above, right*) Native bone. (*Below, left*) Regenerated bone (*red arrow*) formed across the defect site that was filled with a scaffold design that did not include a cap (*blue arrow*). Unoperated bone (*green arrows*) can be seen on either side of the defect site. (*Below, right*) Regenerated bone (*red arrow*) formed across the defect site that was filled with a scaffold design that included a cap (*blue arrow*). Unoperated bone (*green arrows*) can be seen on either side of the defect site.

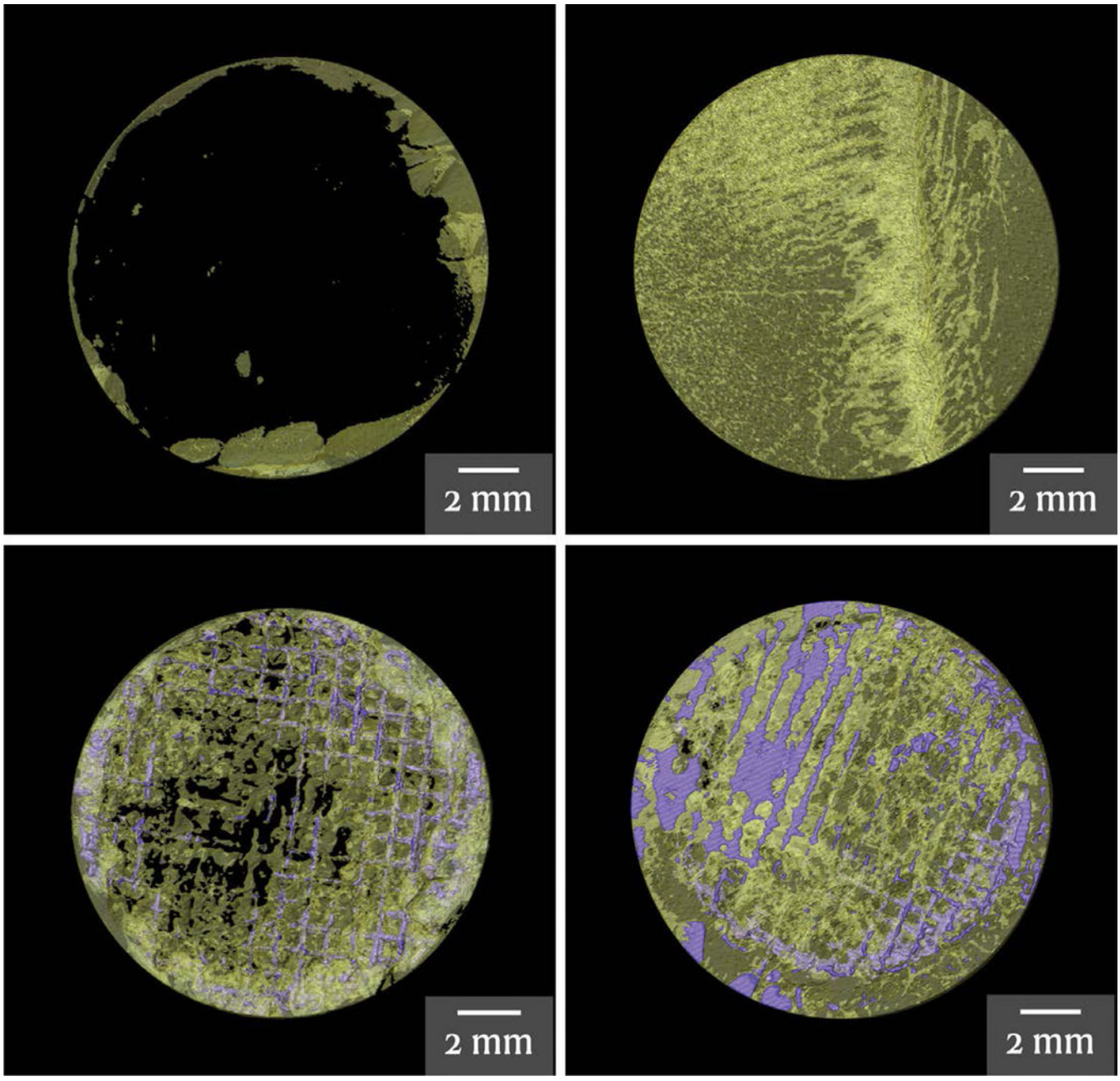


**Fig. 3.**

Three-dimensional reconstruction of the bone (*yellow*) and remaining scaffold (*purple*) in the defect site after 12 weeks of healing in a negative control (*above, left*), a sample of native bone (*above, right*), a defect that had been filled with a scaffold without a cap (*below, left*), and a defect that had been filled with a scaffold with a cap (*below, right*).

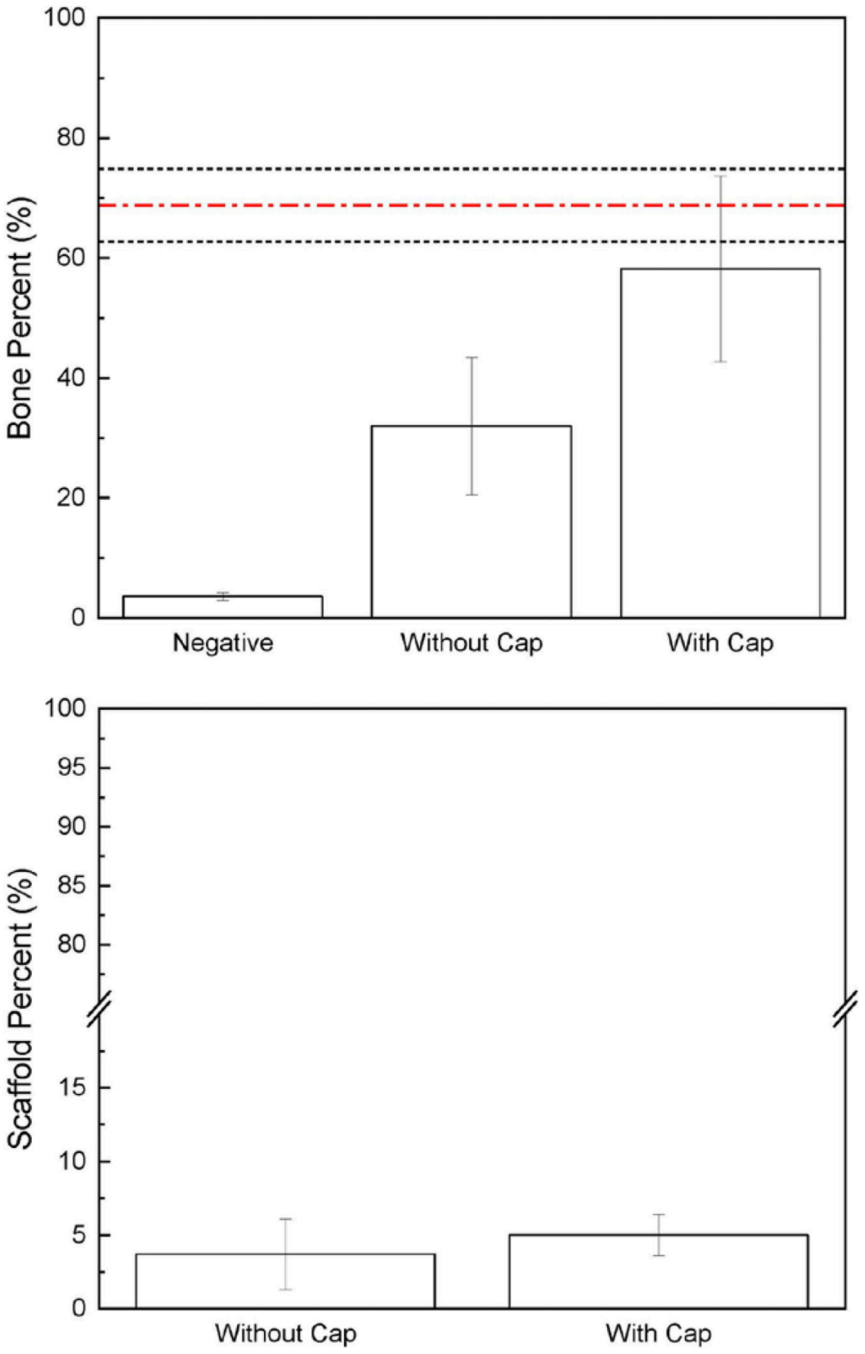


**Fig. 4.**

(*Above*) Bar graph presenting the mean (±SD) of bone that filled the defect sites in each group after 12 weeks of healing compared with the average bone density of native bone (*red line*). The horizontal dashed *red line* denotes the mean with corresponding SD shown by the *black horizontal lines.* (*Below*) Bar graph presenting the averages (±SD) of remaining scaffold in both scaffold design groups after 12 weeks of healing.


**Fig. 5.**

Nondecalcified histologic sections of a negative control after 12 weeks of healing. No bridging bone was seen across any of the unfilled defect sites.

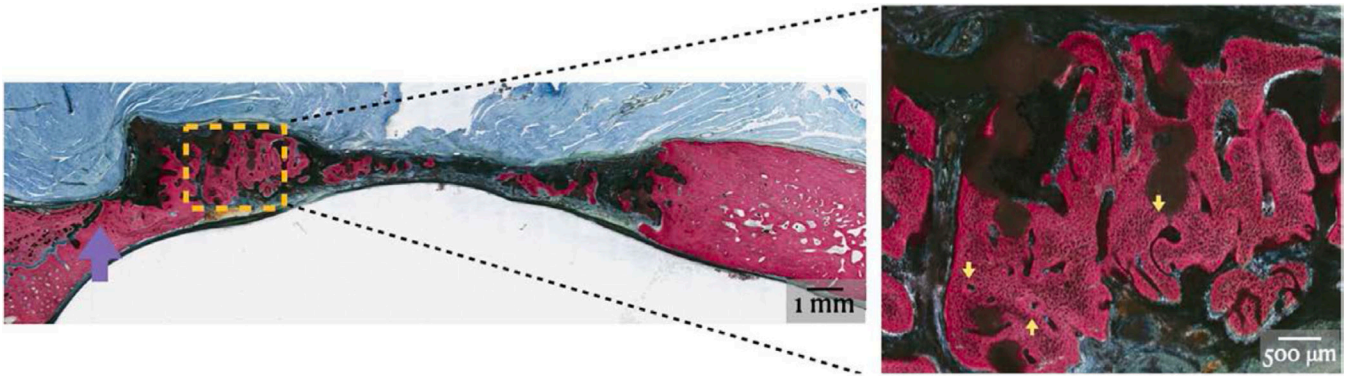


**Fig. 6.**

(*Left*) Nondecalcified histologic section of a defect that had been filled with a scaffold that did not contain a cap after 12 weeks of healing. Vascularized woven and lamellar bone formed throughout the defect site and cranial sutures remained patent (*purple arrow*). (*Right*) Areas of mature, organized bone (*yellow arrows*) can be seen in the higher magnified portion of the slide.

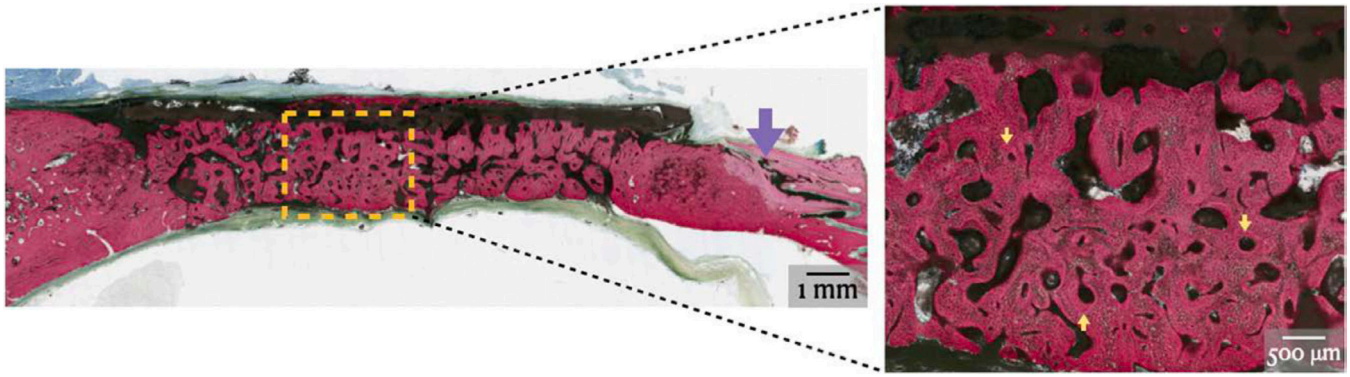


**Fig. 7.**

(*Left*) Nondecalcified histologic section of a defect that had been filled with a scaffold that included a cap after 12 weeks of healing. Vascularized woven and lamellar bone formed throughout the defect site and cranial sutures remained patent (*purple arrow*). (*Right*) Areas of mature, organized bone (*yellow arrows*) can be seen in the higher magnified portion of the slide.

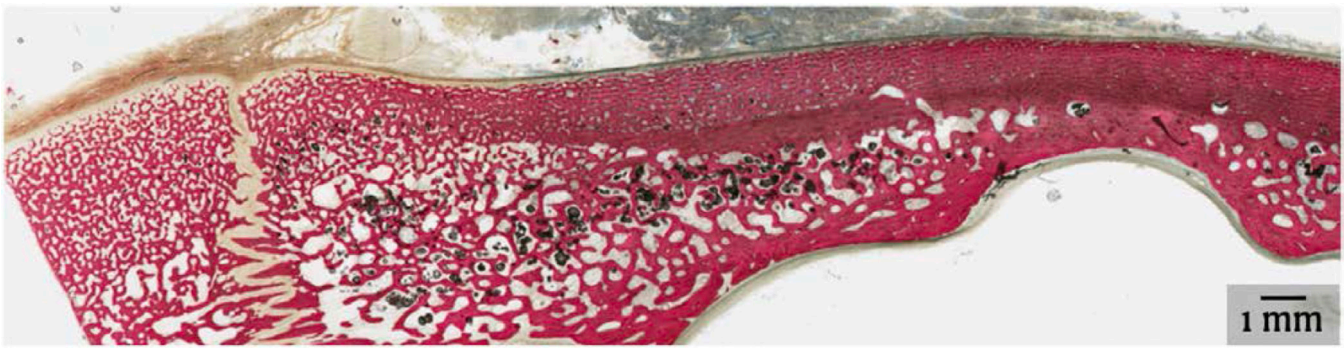


**Fig. 8.**
Nondecalcified histologic section of native bone.

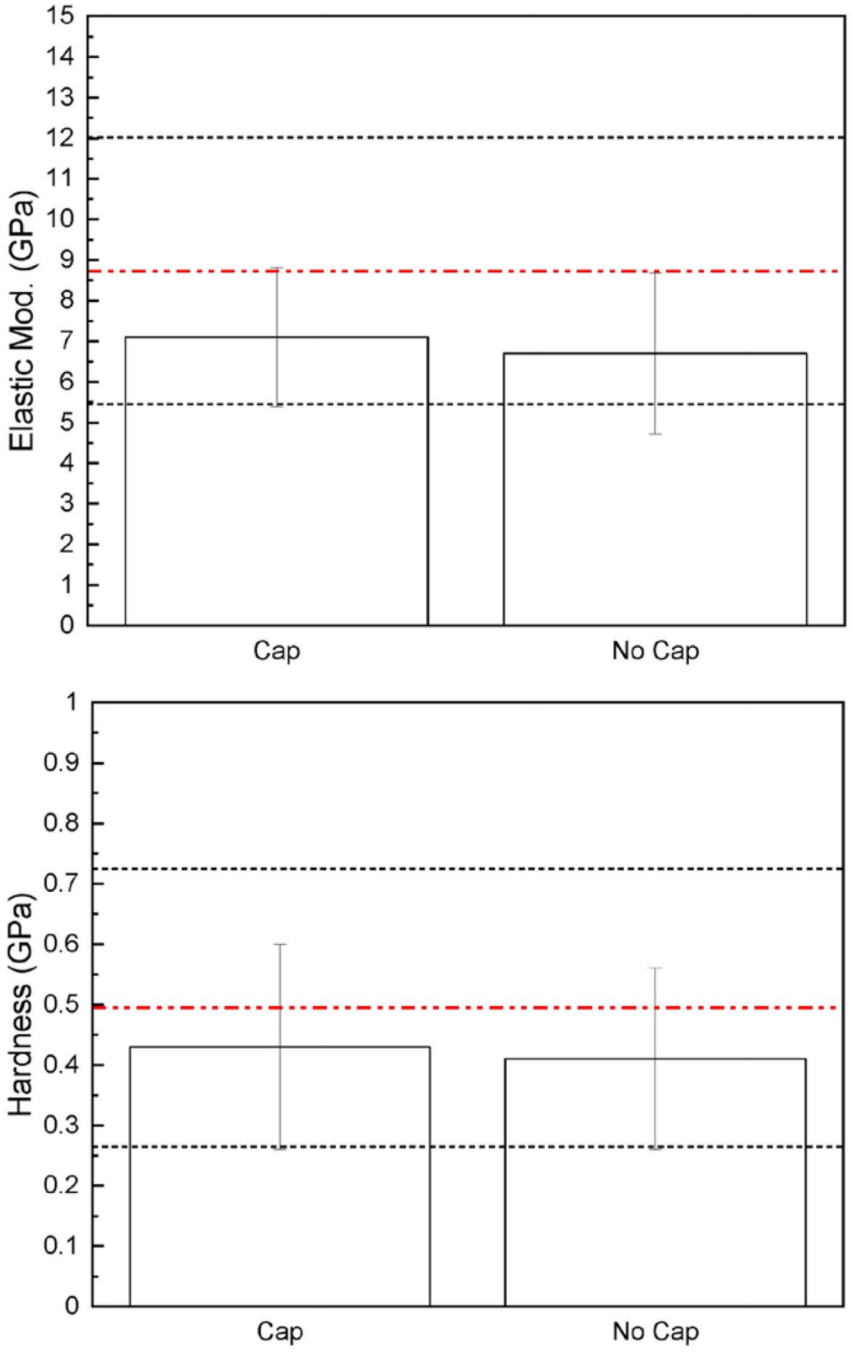


**Fig. 9.**

Bar graphs presenting the mean (±SD) reduced elastic modulus (*above*) and hardness (*below*) of scaffold-regenerated bone in both scaffold design groups compared with native bone (*red line*). The horizontal *dashed red line* denotes the mean with corresponding SD shown by the *black horizontal lines*.

**Table 1.**

Bone and Scaffold Volume Fraction of the Defect Site after 12 Weeks

| | Bone, % (Mean ± SD) | *P* | Scaffold, % (Mean ± SD) | *P* |
|---|---|---|---|---|
| Native bone | 68.8 ± 6.1 | | | |
| Negative control | 3.6 ± 0.7 | ≤0.001 | | |
| Scaffolds (combined) | 45.1 ± 18.9 | | | |
| Without cap | 32.0 ± 11.4 | ≤0.001 | 3.7 ± 2.4 | 0.287 |
| With cap | 58.2 ± 15.5 | | 5.0 ± 1.4 | |